REPORT DOCUMENTATION PAGE

1. REPORT DATE *(DD-MM-YYYY)*	2. REPORT TYPE	3. DATES COVERED *(From - To)*
	Technical Papers	

4. TITLE AND SUBTITLE	5a. CONTRACT NUMBER
Please see attached	
	5b. GRANT NUMBER
	5c. PROGRAM ELEMENT NUMBER

6. AUTHOR(S)	5d. PROJECT NUMBER
	2302
	5e. TASK NUMBER
	M16 2
	5f. WORK UNIT NUMBER
	346120

7. PERFORMING ORGANIZATION NAME(S) AND ADDRESS(ES)

Air Force Research Laboratory (AFMC)
AFRL/PRS
5 Pollux Drive
Edwards AFB CA 93524-7048

8. PERFORMING ORGANIZATION REPORT

9. SPONSORING / MONITORING AGENCY NAME(S) AND ADDRESS(ES)

Air Force Research Laboratory (AFMC)
AFRL/PRS
5 Pollux Drive
Edwards AFB CA 93524-7048

10. SPONSOR/MONITOR'S ACRONYM(S)

11. SPONSOR/MONITOR'S NUMBER(S)

Please see attached

12. DISTRIBUTION / AVAILABILITY STATEMENT

Approved for public release; distribution unlimited.

13. SUPPLEMENTARY NOTES

14. ABSTRACT

20030129 129

15. SUBJECT TERMS

16. SECURITY CLASSIFICATION OF:

a. REPORT	b. ABSTRACT	c. THIS PAGE	17. LIMITATION OF ABSTRACT	18. NUMBER OF PAGES	19a. NAME OF RESPONSIBLE PERSON
Unclassified	Unclassified	Unclassified	A		Leilani Richardson
					19b. TELEPHONE NUMBER *(include area code)* (661) 275-5015

MEMORANDUM FOR PRS (Contractor/In-House Publication)

FROM: PROI (STINFO)   20 Apr 2001

SUBJECT: Authorization for Release of Technical Information, Control Number: **AFRL-PR-ED-TP-2001-100**
Smith, C.W.; Constantinescu, D.M.; Liu, C.T., "Stress Intensity Factor and Paths for Cracks in
Photoelastic Motor Grain Models Under Internal Pressure"

2001 ASME Winter Meeting   (Statement A)
(New York, NY, 5-9 Nov 01)   (Deadline: 24 Apr 01)

1. This request has been reviewed by the Foreign Disclosure Office for: a.) appropriateness of distribution statement,
b.) military/national critical technology, c.) export controls or distribution restrictions,
d.) appropriateness for release to a foreign nation, and e.) technical sensitivity and/or economic sensitivity.
Comments:_____
_____
_____
_____

Signature _____   Date _____

2. This request has been reviewed by the Public Affairs Office for: a.) appropriateness for public release
and/or b) possible higher headquarters review.
Comments: _____
_____
_____
_____

Signature _____   Date _____

3. This request has been reviewed by the STINFO for: a.) changes if approved as amended,
b) appropriateness of references, if applicable; and c.) format and completion of meeting clearance form if required
Comments:_____
_____
_____

Signature _____   Date _____

4. This request has been reviewed by PR for: a.) technical accuracy, b.) appropriateness for audience, c.)
appropriateness of distribution statement, d.) technical sensitivity and economic sensitivity, e.) military/
national critical technology, and f.) data rights and patentability
Comments:_____
_____

APPROVED/APPROVED AS AMENDED/DISAPPROVED

_____
PHILIP A. KESSEL   Date
Technical Advisor
Space and Missile Propulsion Division

STRESS INTENSITY FACTORS AND PATHS FOR CRACKS IN PHOTOELASTIC MOTOR GRAIN MODELS UNDER INTERNAL PRESSURE

C. W. Smith*,
D. M. Constantinescu* and C. T. Liu[‡]

* Department of Engineering Science and Mechanics
Virginia Polytechnic Institute and State University
Blacksburg, VA 24061

[‡] Air Force Research Laboratory, PRSM
10 E. Saturn Blvd.
Edwards, AFB, CA 93524-7680

ABSTRACT

Computational analysis and two-dimensional tensile tests on single motor grain fins suggest that cracks in fin tips are most likely to originate at the coalescence of a fin end tip radius, with a small radius from the side of the fin. Some manufacturers have also noticed defects formed during casting at the fin tip on the fin axis. The following is an experimental investigation utilizing frozen stress photoelastic models of an existing motor grain geometry in order to clarify stress intensity factor (SIF) values and crack growth paths for cracks emanating from the two above- noted potential critical loci. Comparisons between results from cracks grown from the two loci will be made, suggesting interesting conclusions.

INTRODUCTION

Two-dimensional thermal shrinkage tests on photoelastic models and two-dimensional tensile tests on single fin sections of motor grain have suggested that, for a specific fin geometry consisting of a small edge fin radius coalescing into a large fin tip radius, the critical locus for crack initiation lies at the point of confluence for the two radii at the fin tip. On the other hand, some motor grain manufacturers have reported cracks emanating from the fin tip along its own axis of symmetry as a result of voids collecting there during the casting process. One aspect of the problem which has not been explored is how cracks would grow from these two critical points in a three-dimensional model and the corresponding stress intensity factors.

The first author and his colleagues have achieved some success (Smith, 1990), (Smith and Wang, 1992), (Smith, Wang and Liu, 1995), (Smith, Liu and Wang, 1995) combining the frozen stress photoelastic method (Appendix A) together with a two-parameter method (Smith and Kobayashi, 1993) for analyzing local stress fields around crack tips for (SIF) determination in generic and specific rocket motor geometries. The present paper describes an attempt to use this method to study the crack growth and SIF values for cracks emanating from the two critical loci described above in three-dimensional models under internal pressure.

TEST MODELS AND PROCEDURES

All tests models were cast at Measurements Group (Raleigh, NC) in molds provided by Virginia Tech using PLM-4BR stress freezing material manufactured by Measurements Group. The model dimensions are pictured in Fig. 1. The starter

cracks were made by first drilling a small hole opposite the fin in which the crack was to be located, sliding a shaft with a tip blade into the hole, positioning the blade at the critical point on the fin surface and then striking the shaft with a hammer. The starter cracks then emanated from the blade tip into the material as "natural" or real cracks. For the cracks located at the point of confluence of the small fin edge radius with the larger fin tip surface radius, a shorter tip blade was used opposite the main blade to balance the impact load on the shaft (Fig. 2). This shorter blade caused some slight damage and sometimes a small crack which was patched with PMC-1 cement. Of course, cracks emanating from the critical locus on the axis of symmetry required no balance blade and were more easily produced. After the starter cracks were made, the drilled holes were plugged and sealed.

It is important that crack growth be achieved from these starter cracks under pressure in order to establish the "pressure" crack growth path as opposed to the starter crack generated by wedge forces.

The test setup is pictured in Fig. 3. The pressure was monitored only outside the model, as indicated, and maintained its value when end caps leaked or when a crack grew through the model wall. In addition to the internal pressure, an end load was applied to the model to approximately simulate the effect of an open end as the motor grain may experience in service.

Four identical models have been tested to date. Model #1 was utilized solely to determine the stress fringe order at the two critical loci without cracks (Fig. 4). Since the test material showed a slight deterioration in the surface layer, graphs of fringe order versus path along "squeezed" fringes were extrapolated to the boundary and showed little difference in fringe value at the two critical points (Fig. 5).
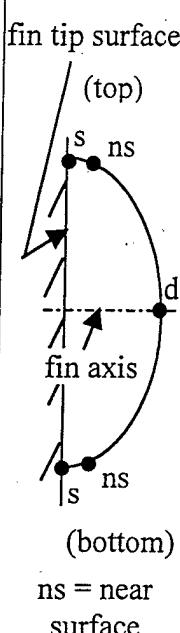
Models #2, #3 and #4 each contained two cracks; in each case in fins adjacent to an uncracked fin and one with a plugged hole in order to allow independent analysis at each crack (Fig. 6). After stress freezing and removal of thin slices mutually orthogonal to the local crack surface and its border, the slices were analyzed by a two-parameter model, briefly described in Appendix B.

RESULTS

As noted above, two types of cracks were used in the experiments. Cracks which were symmetric with respect to both load and geometry were initiated at the fin tip along the axis of the fin. These cracks were planar, semi-elliptic cracks which maintained these characteristics as they grew. SIF values were determined at maximum depth, along or near to the fin surface, and exhibited pure Mode I SIF values. Two of these cracks penetrated the outer surface of a model and readily grew at smaller load levels than the off-axis cracks which emanated at the locus of confluence of the two fin tip radii. These off-axis cracks were generally non-planar and were extremely difficult to grow even at elevated pressures. This was because the tips of these cracks were under mixed mode load and had to turn a significant amount in order to grow. In fact, with one exception, none of these cracks reached a purely Mode I state during testing.

The test data and results are presented in a normalized form in Table I. Since stress freezing pressure was maintained after breakthrough, data did not appear to be adversely affected. However, fringe observations on Model 1 and SIF data on one end of the long

Table I

Loads[1]	Crack Description[2]	depth (d)	surface (s) top	surface (s) bottom	
		$F_i = K_i\sqrt{Q}\big/ p_{sf}\sqrt{\pi a^3}$ $i = 1, 2$			
Model 2					fin tip surface (top)
$P = 311.4$ N $p_{max} = 0.145$ MPa $p_{sf} = 0.07$ MPa	Long off-axis crack $a/c = 0.66$ $a/t = 0.26$	$F_1 = 2.03$ $F_2 = 0$	2.42	2.90	
	Long symmetric crack $a/c = 0.9$ $a/t = 1.0$	penetrated	—	2.72	
Model 3					fin axis
$P = 311.4$ N $p_{max} = 0.103$ MPa $p_{sf} = 0.033$ MPa	Short symmetric crack $a/c = 0.5$ $a/t = 0.41$	1.67	2.25	1.82	
	Long symmetric crack $a/c = 0.68$ $a/t = 1.0$	penetrated	2.00	2.16	(bottom) ns = near surface
Model 4					t = distance from fin tip to outer surface along fin axis, (37.08 mm)
$P = 88.97$ N $p_{max} = 0.049$ MPa $p_{sf} = 0.035$ MPa	Right off-axis $a/c = 0.81$ $a/t = 0.25$	$F_1 = 1.51+$ $F_2 = 0.47+$	—	—	
	Left off-axis $a/c = 0.78$ $a/t = 0.23$	$F_1 = 1.90$ $F_2 = 0.48$	ns 2.62	ns 2.55	

+ Opposite crack surfaces were not uniformly separated through the slice and this led to local fringe distortions.

Notations:

1 - P = axial compressive load

p_{max} = maximum internal pressure to grow crack

p_{sf} = stress freezing pressure

2 - a = crack length

c = half length of crack in fin tip surface

3 - $\sqrt{Q}$ = approximation of elliptic integral of second kind

$$Q = 1 + 1.464\left(\frac{a}{c}\right)^{1.65} \qquad \frac{a}{c} \leq 1$$

$$Q = 1 + 1.464\left(\frac{c}{a}\right)^{1.65} \qquad \frac{a}{c} > 1$$

All flaws were characterized as semi-elliptic flaws of depth a and length $2c$. However, off-axis cracks were neither perfectly semi-elliptic nor planar.

symmetric crack in Model 2, together with surface values for the right off-axis crack in Model 4, suggested a small skin effect in the material, so these values were omitted. In order to escape this effect, values of F_1 were obtained 20° off of the surface or near the fin surface "ns" in Model 4 and appeared quite reasonable. All of the cracks grew more along the axis of the model than through the thickness.

The long off-axis crack in Model 2 was the only such crack to grow sufficiently to escape the shear mode. It is pictured in Fig. 7.

SUMMARY

Based on the above studies to date, it has been found that:

i. Cracks emanating from a fin tip on the axis of the fin exhibit pure Mode I and grow more readily than those emanating from the point of confluence of tip radii.

ii. Cracks emanating from the confluence of tip radii exhibit mixed mode conditions around the crack front and maintain a mixed mode condition as the crack front turns, exhibiting strong resistance to further crack growth.

iii. Normalized stress intensities based upon a planar semi-elliptic shape are computed at maximum depth and near the fin surface.

iv. While cracks emanating from the fin tip on the axis of symmetry remain essentially planar, the off-axis cracks generate curved surfaces.

The preliminary study described above suggests that the use of off-axis cracks may be an unnecessary complication in predicting crack growth and SIF determination due to the substantial irregularities and highly elevated loads required to induce sufficient crack growth in off-axis cracks to shed the shear mode for the geometry studied. However, further experiments are underway in order to further extend the results.

REFERENCES

Smith, C. W., "Fracture Parameter Measurements for Cracks Emanating from Curved Surfaces by the Frozen Stress Method," *Proc. of 9th International Conference on Experimental Mechanics,* Vol. 5, pp. 1776-1785, (1990).

Smith, C. W., and Wang, L., "Stress Intensity Factor Distribution and Crack Shapes in 3-D Problems Using Frozen Stress," *Advances in Local Fracture/Damage Models for the Analysis of Engineering Problems,* ASME-AMD-Vol. 137, pp. 109-120, (1992).

Smith, C. W. and Kobayashi, A. S., "Experimental Fracture Mechanics," Chapter 20: *Handbook on Experimental Mechanics,* 2nd Ed., Kobayashi, A. S., Ed. VCH New York, pp. 905-968, (1993).

Smith, C. W., Wang, A. L. and Liu, C. T., "Experimental Determination of Crack Growth Paths and SIF Distributions in Motor Grain Geometries," *Proc. of 1995 Society for Experimental Mechanics Spring Conference,* pp. 139-145, (1995).

Smith, C. W., Liu, C. T., and Wang, A. L., "Crack Growth and SIF Distributions at Critical Locations in Scale Models of Motor Grain Using Frozen Stress," *Recent Advances in Solids and Structures,* ASME PVP Vol. 321/NE Vol. 18, pp. 19-24, (1995).

APPENDIX A- Frozen Stress Photoelasticity

When a transparent model is placed in a circularly polarized monochromatic light field and loaded, dark fringes will appear which are proportional to the applied load. These fringes are called stress fringes or isochromatics, and the magnitude of the maximum in-plane shear stress is a constant along a given fringe.

Some transparent materials exhibit mechanical diphase characteristics above a certain temperature, called the critical temperature (T_c). The material, while still perfectly elastic, will exhibit a fringe sensitivity of about twenty times the value obtained at room temperature, and its modulus of elasticity will be reduced to about one six-hundredth of its room temperature value. By raising the model temperature above T_c, loading, and then cooling slowly to room temperature, the stress fringes associated with T_c will be retained when the material is returned to room temperature. Since the material is so much more sensitive to fringe generation above T_c than at room temperature, fringe recovery at room temperature upon unloading is negligible. The model may then be sliced without disturbing the "frozen in" fringe pattern and analyzed as a two-dimensional model but containing the three-dimensional effects. In the use of the method to make measurements near crack tips, due to the need to reduce loads above critical temperature to preclude large local deformations, and the use of thin slices, few stress fringes are available by standard procedures. To overcome this obstacle, a refined polariscope is employed to allow the tandem use of the Post and Tardy methods to increase the number of fringes available locally.

In fringe photographs, integral fringes are dark in a dark field and bright in a bright field. Bright fields are used throughout this paper.

APPENDIX B

MODE I ALGORITHM

Beginning with the Griffith-Irwin Equations, we may write, for Mode I, for the homogeneous case,

$$\sigma_{ij} = \frac{K_1}{(2\pi r)^{\frac{1}{2}}} f_{ij}(\theta) + \sigma_{ij}^{\circ} \qquad (i,j = n,z) \quad (1)$$

where:

σ_{ij} are components of stress

K_1 is SIF

r, θ are measured from crack tip (Fig. B-1)

σ_{ij}° are non-singular stress components.

Then, along $\theta = \pi/2$, after truncating σ_{ij}

$$\tau_{nz}^{\max} = \frac{K_1}{(8\pi r)^{\frac{1}{2}}} + \tau^{\circ} = \frac{K_{AP}}{(8\pi r)^{\frac{1}{2}}} \qquad (2)$$

where: $\tau^{\circ} = f(\sigma_{ij}^{\circ})$ and is constant over the data range

K_{AP} = apparent SIF

$\tau_{nz}^{\max}$ = maximum shear stress in nz plane

$$\therefore \frac{K_{AP}}{\bar{\sigma}(\pi a)^{\frac{1}{2}}} = \frac{K_1}{\bar{\sigma}(\pi a)^{\frac{1}{2}}} + \frac{\sqrt{8}\tau^{\circ}}{\bar{\sigma}} \left(\frac{r}{a}\right)^{\frac{1}{2}} \qquad (3)$$

where (Fig. B-1) a = crack length, and $\bar{\sigma}$ = remote normal stress

i.e. $\dfrac{K_{AP}}{\bar{\sigma}(\pi a)^{\frac{1}{2}}}$ vs. $\sqrt{\dfrac{r}{a}}$ is linear.

Since from the Stress-Optic Law

$$\tau_{nz}^{\max} = \frac{nf}{2t} \text{ where}$$

n = stress fringe order

f = material fringe value

t = specimen (or slice) thickness

and from Eq. 2

$$K_{AP} = \tau_{nz}^{max}(8\pi r)^{\frac{1}{2}} = \frac{nf}{2t}(8\pi r)^{\frac{1}{2}},$$

then K_{AP} (through a measure of n) and r becomes the measured quantity from the stress fringe pattern at different points in the pattern.

In the present study, instead of normalizing K with respect to $\overline{\sigma}(\pi a)^{1/2}$, we have selected $p\sqrt{\pi a/Q}$ as the normalizing factor where $\sqrt{Q}$ is an elliptic integral of the second kind approximated here, as shown in Table I. An example of the determination of F_1 in Table I from test data is given in Fig. B-2.

MIXED MODE ALGORITHM

The mixed mode algorithm was developed (see Fig. B-3) by requiring that:

$$\lim_{\substack{r_m \to 0 \\ \Theta_m \to \Theta_m^\circ}} \left\{ (8\pi r_m)^{1/2} \frac{\partial(\tau_{nz}^{max})}{\partial\Theta}(K_1, K_2, r_m, \Theta_m, \tau_{ij}) \right\} = 0$$

$$(4)$$

which leads to:

$$\left(\frac{K_2}{K_1}\right)^2 - \frac{4}{3}\left(\frac{K_2}{K_1}\right)cot2\Theta_m^\circ - \frac{1}{3} = 0 \qquad (5)$$

By measuring Θ_{m}° which is approximately in the direction of the applied load, K_2/K_1 can be determined.

Then writing the stress optic law as:

$$\tau_{nz}^{max} = \frac{fn}{2t} = \frac{K_{AP}^*}{(8\pi r)^{\frac{1}{2}}}$$

one may plot $\dfrac{K_{AP}^*\sqrt{Q}}{p\sqrt{\pi a}}$ vs. $\sqrt{r/a}$ as before, locate a linear zone and extrapolate to $r = 0$ to obtain K^*. Now K^*, may be written as:

$$K^* = [(K_1 sin\Theta_m^\circ + 2K_2 cos\Theta_m^\circ)^2 + (K_2 sin\Theta_m^\circ)^2]^{\frac{1}{2}} \quad (6)$$

Knowing K^* and θ_m°, K_1 & K_2 can be determined from Eqs. 5 and 6. Details are found in Smith and Kobayashi (1993).
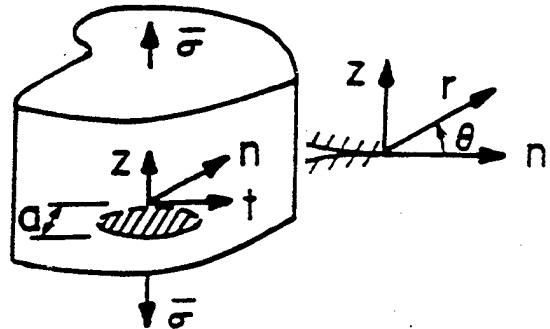

Fig. B-1 Near Tip Notation for Mode I

Model 3, short symmetric crack,
a/c = 0.5, a/t = 0.41, depth (d)

$y = 5.43x + 1.67$

$F_1 = \frac{K_1\sqrt{Q}}{p\sqrt{\pi a}}$
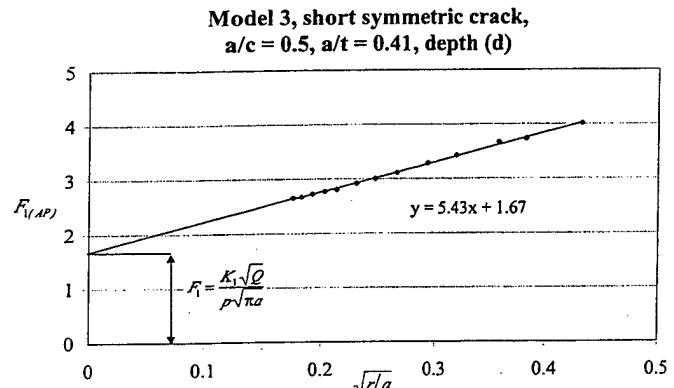
Fig. B-2 Determination of F_1 from Test Data

Fig. B-3 Determination of θ_m° for Mixed Mode

length of cylinder 376 mm

all dimensions are in mm
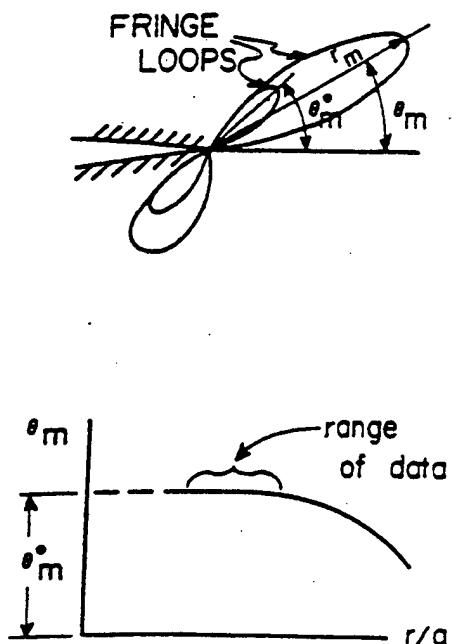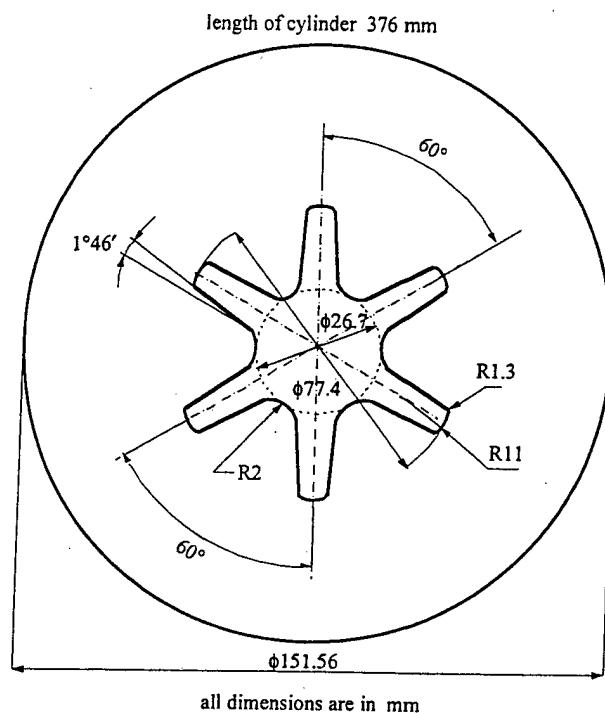
Fig. 1 Model Dimensions
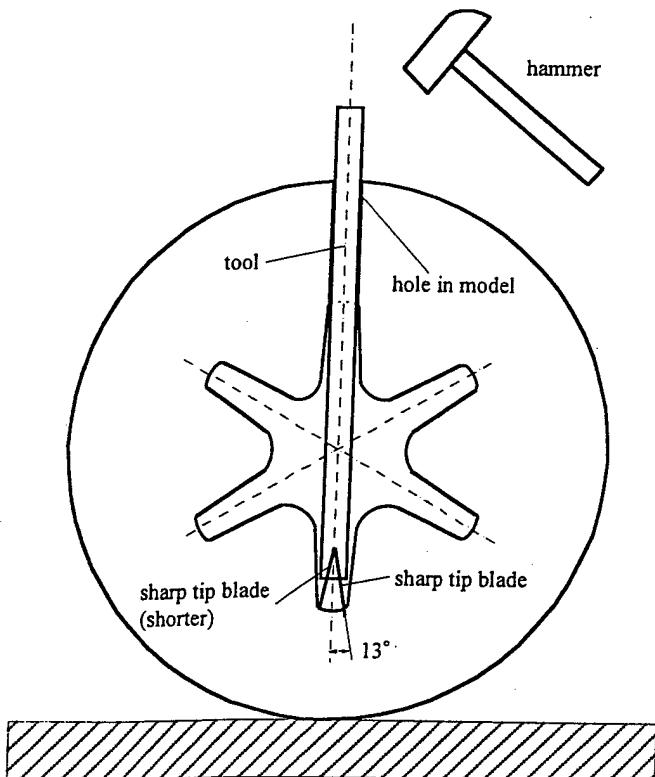
Fig. 2 Setup for Producing Off-Axis Starter Crack

oven

dead weight

RTV rubber cap

$\phi151.56$

model

376

tight fit

RTV rubber cap

loose fit

$\phi6.35$ Copper tube

458x356x12.7 Al plate

all dimensions are in mm

Al collar

230 °F

Al collar

70 °F

oven base

$\phi6.35$ Copper tube to precision pressure gage
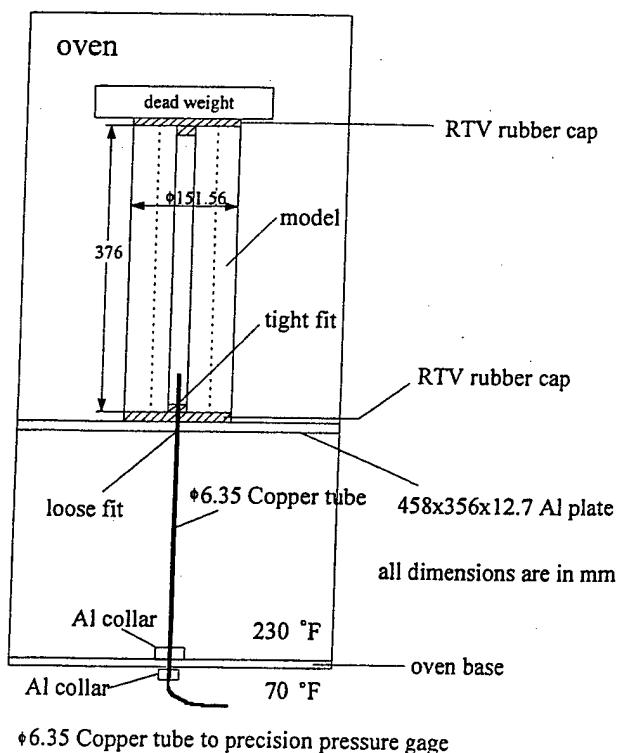
Fig. 3 Stress Freezing Test Setup
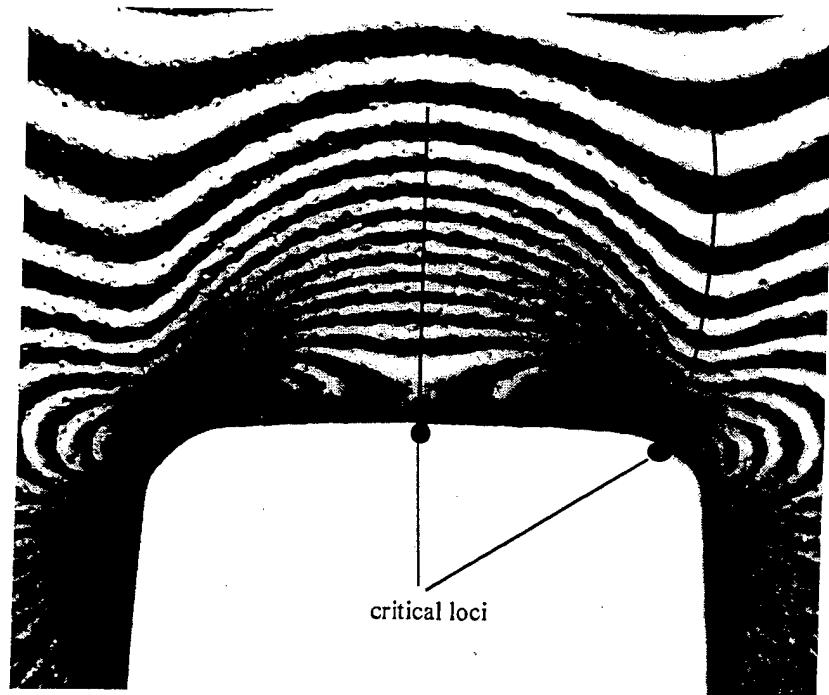
critical loci

Fig. 4 Fringe Patterns Near Critical Loci at Fin Tip

fringe order estimation along the axis of symmetry and off-axis of symmetry around the fin tip

- ♦ axis of symmetry fringe order
- ■ off-axis of symmetry fringe order

$y = 0.5948x^2 - 4.9986x + 20.661$

off-axis measurement is the average of the left and right
minimum location of fringe order

fringe order (N)

distance from fin tip (mm)
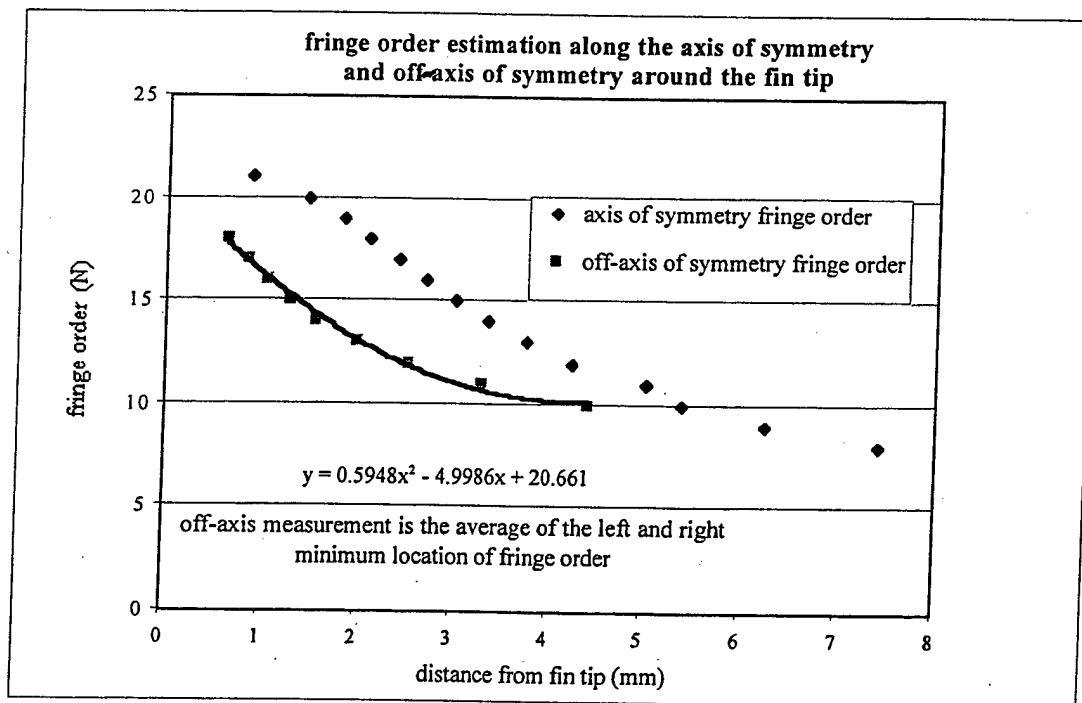
Fig. 5 Convergence of Fringe Orders at Critical Loci in Uncracked Fin

Crack*

Fin tip

Plug

Fin axes

Crack*

Plug

Fin tip
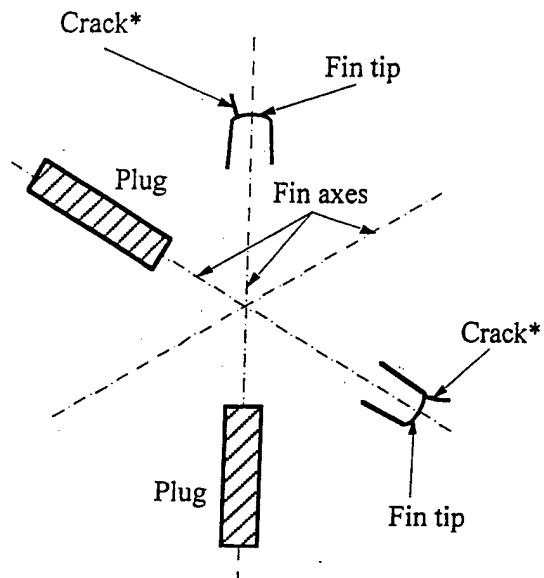
* Path of crack to maximum depth

Fig. 6 Locations of Cracks in Model

section S – S   D – camera view of the photograph   S   Slices normal to photo through A, C', C''
                                                                          were used to determine K

A

C   F   I

D

C'   FS   C''

CFS

CFS – corner of fin surface   I – initial crack   S
C – crack front   F – final crack   FS – fin surface

MF = 4.46
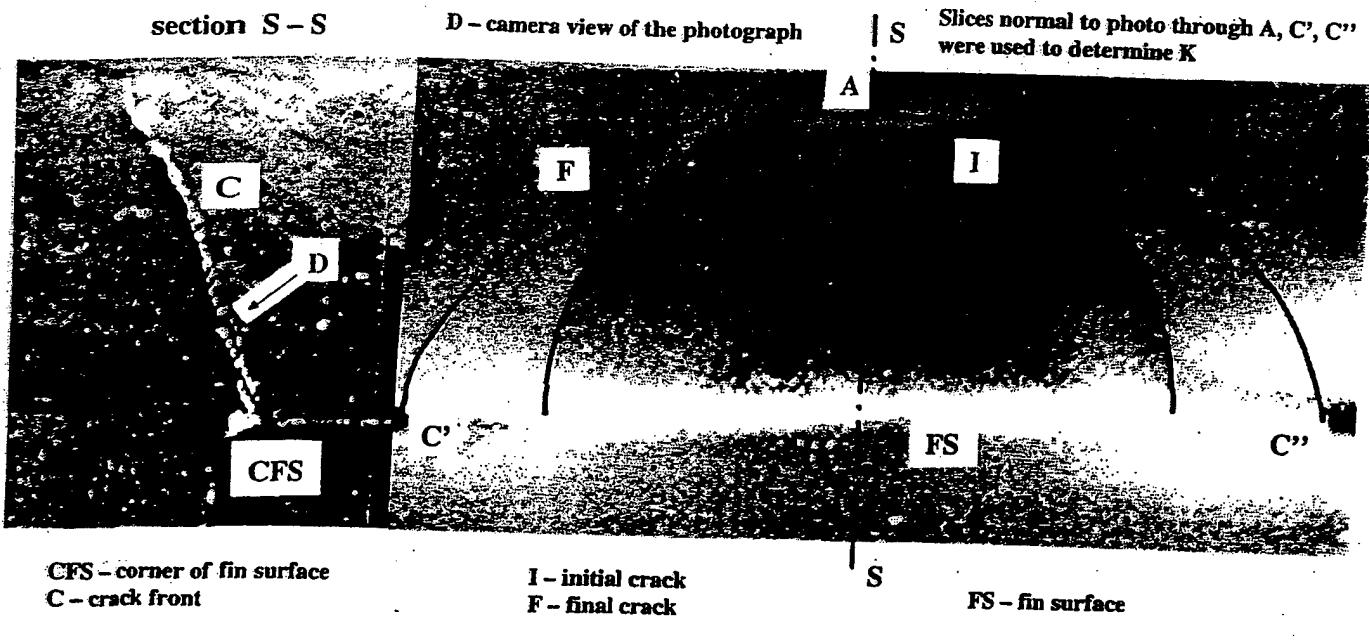
Fig. 7 A Long Off-Axis Crack (Model 2)